

Research Article

Optical and Mössbauer spectroscopy of lithium tetraborate glass doped with iron oxide



Essam A. Elkelany^{a,*}, Moukhtar A. Hassan^b, A. Samir^c, A.M. Abdel-Ghany^a, H. H. El-Bahnasawy^b, M. Farouk^{b,**}

^a Basic Science Department, Faculty of Engineering, Sinai University, Al-Arish, 45511, Egypt

^b Physics Department, Faculty of Science, Al-Azhar University, Cairo, 11884, Egypt

^c Engineering Mathematics and Physics Department, Faculty of Engineering at Shoubra, Benha University, 11629, Egypt

ARTICLE INFO

Keywords:

Ligand field
Borate glasses
Mössbauer spectroscopy
FTIR and ESR spectra

ABSTRACT

The glass system with composition $[80\text{Li}_2\text{B}_4\text{O}_7 + (20-x)\text{ZnO} + x\text{Fe}_2\text{O}_3]$ where $x = (0, 2, 4, 6, 8 \text{ mol. } \%)$, was prepared by traditional melt quenching method. The impact of iron ions on the structural and optical properties of the investigated samples was studied by a set of commentary techniques including density, infrared, optical absorption, electron spin resonance (ESR) and Mössbauer measurements. The obtained results indicate that both the measured density and calculated molar volume increase with Fe_2O_3 content. IR spectra revealed the characteristic absorption bands of BO_3 and BO_4 structural units. The optical absorption spectra of the glass samples featured four bands which are characteristic of Fe^{3+} in tetrahedral (Td) symmetry. The ligand field strength (10Dq), Racah parameters (B and C) and nephelauxetic effect (h) were calculated. ESR spectra were consistent with the optical findings, showing a broad resonance signal at $g \sim 2.1$, sharp signal at $g \sim 4.1$ and tiny shoulder (kink) at $g \sim 6.7$. Mössbauer spectra show two phases of iron ions existing within the glass network, the first is related to Fe^{3+} ions in octahedral (Oh) sites with the isomer shift $(0.675\text{--}0.553) \text{ mm s}^{-1}$, the second is related to Fe^{3+} ions in Td sites with the isomer shift below 0.34 mm s^{-1} .

1. Introduction

Glasses doped with transition metal ion find interesting technological applications [1]. B_2O_3 is one of the most important glass formers. It is a particularly suitable optical material because of its high thermal stability, high chemical, mechanical strength and low melting point [2]. Two forms of boron coordination BO_3 and BO_4 have been reported and the conversion of BO_3 into BO_4 units and vis versa depends on the concentration, nature and type of the added modifiers [3]. $\text{Li}_2\text{B}_4\text{O}_7$ have a good deal of interest owing to its non-linear optical properties and broad transmission window [4]. In addition, it is employed in many interesting applications such as radiation resistance of optical materials, radiation dosimetry [5]. ZnO enters the host matrix of the glass in the form of both network former and modifier. Specifically, ZnO acting as a network modifier is known to significantly modify different glass properties [6–8]. Borate glass containing Fe_2O_3 has a great importance owing to its manifold applications such as electronic, electrochemical,

electro-optic devices and photo catalyst [9]. Iron has different redox states, where it is mostly present in the glass matrices in Fe^{2+} or/and Fe^{3+} states [1,10]. Fe^{3+} ion has a $3d^5$ configuration and the spin-allowed transitions are not available for d^5 configuration (spin-forbidden) [11]. The spin-forbidden transitions of d^5 configuration of Fe^{3+} ions become allowed by the magnetic coupling of electronic spin of next-nearest neighbor Fe^{3+} ions in the structure. Also, the spin-forbidden transitions may occur by vibronic coupling, which includes coupling of vibrational and electronic wave functions with opposite parities [11, 12]. When iron ions are surrounded with a ligand field, the 3d orbitals split into two groups (t_2 and e , when the ions occupy the Td coordination positions. or t_{2g} and e_g , when the ions occupy the Oh coordination positions.). The energy separating between the two groups is called as the ligand field strength (10Dq), the electronic transition between the states of the two groups is called the ligand field transition. The energies of these states are expressed in terms of three parameters; Racah parameters (B, C) and 10Dq [12–14]. ESR is an effective technique for the

* Corresponding author.

** Corresponding author.

E-mail addresses: Essamelkelany88@gmail.com (E.A. Elkelany), m_farouk@azhar.edu.eg (M. Farouk).

examination of local structure and paramagnetic centers of transition metal doped oxide glasses [15,16]. Iron ions have two valence states within the glass network, trivalent state Fe^{3+} and bivalent state Fe^{2+} . ESR exhibits trivalent state Fe^{3+} only at RT [10]. Mössbauer spectroscopy is most effective technique to study the coordination number and valence state of iron. Mössbauer's parameters reflect the hyperfine interactions between Mössbauer's nucleus atom and its surrounded electrons as well as the effect of ligand on distribution of the electrons [17–19]. To the best of our knowledge, there are no previous works were done to study the ligand field parameters of borate glasses doped with Fe ions by derived mathematical equations from Tanabe-Sugano expressions for the ligand field state energies. Therefore, the purpose of this work is to study the effect of Fe_2O_3 on the structural and optical properties of the glass system $[\text{80Li}_2\text{B}_4\text{O}_7 + (20-x)\text{ZnO} + x\text{Fe}_2\text{O}_3]$ with $x = (0, 2, 4, 6$ and 8 mol. %), to shed some light on the optical transitions of Fe^{+3} ions trying to show them clearly in UV–Vis–NIR spectrum and to calculate 10Dq and Racah parameters (B, C) using mathematical equations derived from Tanabe-Sugano expressions for the ligand field state energies.

2. Experimental details

The glass system $80\text{Li}_2\text{B}_4\text{O}_7 + (20-x)\text{ZnO} + x\text{Fe}_2\text{O}_3$ where $x = (0, 2, 4, 6$ and 8 mol. %), was produced by normal melt quench method. The glass samples were labeled Fe glasses; Fe0, Fe2, Fe4, Fe6, Fe8 corresponding to $x = 0, 2, 4, 6, 8$, respectively. The raw chemical materials were mixed and milled to reach the homogeneity; the homogeneous mixtures were put in porcelain melting pots for 1 h in an electrical oven at 1373 K. During the melt, the molten mixtures were swirled for complete homogenization, finally the melts were rapidly quenched at room temperature (RT). The obtained Fe glass samples are homogeneous, transparent, and colored as shown in Fig. 1. Density (ρ) of the Fe glasses was measured at RT employing Archimedes method, where Carbon tetrachloride (CCl_4) was used as an immersion liquid. Infrared (IR) absorption spectra of the Fe glasses in the range $400\text{--}1600\text{ cm}^{-1}$ were performed employing KBr pellets technique using Thermo FT-IR 200 spectrometer. UV–Vis–NIR absorption spectra of the Fe glasses from 190 to 1100 nm were performed at RT using JASCO V-670 UV–Vis spectrophotometer. ESR spectra of Fe glasses (powder) were carried out at RT using EMX-Bruker X-band ESR spectrometer with 10 mW microwave power and 100 kHz field modulation. ^{57}Fe -Mössbauer spectra of the Fe doped glass samples were gathered at RT by the constant acceleration mode with a ^{57}C source diffused in a Rh matrix and $\alpha\text{-Fe}$ was used for spectrometer calibration.

3. Results and discussion

3.1. Infrared spectra

IR spectra can provide us with some information about the vibrational modes as a result of specific chemical bonds in molecule. The IR spectra of borate glass consist of three main regions. The first region is located in the range $(600 - 800)\text{ cm}^{-1}$ is related to the B–O–B bending vibration modes of (BO_3) units. The second region in the range $(800 - 1200)\text{ cm}^{-1}$ is correlated to the B–O bond stretching in (BO_4) units. The third region vibrates in the range $(1200 - 1600)\text{ cm}^{-1}$ is related to stretching of the B–O in $(\text{BO}_3, \text{BO}_2\text{O}^-)$ units [3,20,21]. Sometimes, these regions displace to higher/lower wavenumbers depending on the glass system [3]. The spectra of the Fe glasses with different rates of Fe_2O_3

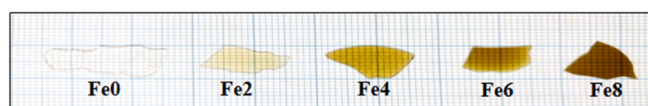


Fig. 1. Fe glass samples.

content exhibited four fundamental bands at $\sim 400, \sim 694, \sim 962,$ and 1370 cm^{-1} . A tiny band appears clearly at around 623 cm^{-1} with addition Fe_2O_3 to the glass composition, which may be attribute to iron ions, as shown in Fig. 2. The band at $\sim 400\text{ cm}^{-1}$ is related to vibration mode of Li–O and Zn–O [8,22]. In addition, the band at $\sim 694\text{ cm}^{-1}$ is related to symmetric bending vibration mode of B–O–B in BO_3 unit [4, 22,23]. Additionally, the band at $\sim 962\text{ cm}^{-1}$ is related to stretching vibration mode of B–O and rocking vibrations of BO_4 units [22,23]. Moreover, the band at $\sim 1370\text{ cm}^{-1}$ is related to stretching vibration mode of B–O in BO_3 units [9,21,24,25]. The band at $\sim 623\text{ cm}^{-1}$ is due to overlap of Fe–O stretching vibration in FeO_4 units [24,26,27] with B–O–B bending vibration in BO_3 units as well as deformation modes of borate rings [4,21–23]. A deconvolution process carried out for the bands of IR spectra using Gaussian function to get a deeply explanation of the spectra (not shown). The peaks of deconvoluted bands were mentioned in Table 1.

The fraction of four coordination boron atoms were calculated according to the relation [4]:

$$N_4 = \frac{A_4}{A_4 + A_3} \quad (1)$$

where A_4 and A_3 are the area under the peaks of BO_4 and the area under the peaks of BO_3 , respectively. In the studied system, the obtained values of N_4 were indexed in Table 1. The decreasing of N_4 values as Fe_2O_3 content increase, is due to the transformation of BO_4 to BO_3 and creating of non-bridging oxygen's (NBOs), this change lower the stability of the glass [8]. The increasing in intensities and average area of two NBOs peaks at 867 cm^{-1} and 1238 cm^{-1} show an enhancement of NBOs bonds in glass matrix as Fe_2O_3 content increase. The variation of N_4 and average NBOs ratio as a function of Fe_2O_3 content is illustrated in Fig. 3.

3.2. Physical properties

The density (ρ) of the prepared glass samples increases as Fe_2O_3 content increase at the expense of ZnO from 2.457 g/cm^3 to 2.483 g/cm^3 . The noticeable augmentation in density values may be as a result of the molecular weight of Fe_2O_3 (159.687 g/mol) is larger than that of ZnO (81.389 g/mol). The molar volume (V_m) of the samples was computed through the following equation [28]:

$$V_m = M_T / \rho \quad (2)$$

where M_T is the total molecular weight. The V_m of the Fe glasses increases from $61.689\text{ cm}^3/\text{mol}$ to $63.560\text{ cm}^3/\text{mol}$ with the increment of

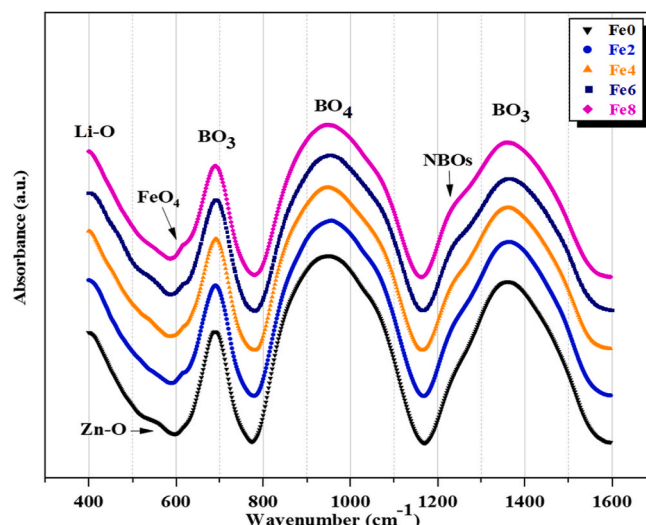


Fig. 2. The IR absorption spectra of all glass samples.

Table 1
Peak positions, assignments and N_4 of IR absorption spectra of Fe glass samples.

Peak No	Wavenumber (cm^{-1})					Assignment (vibration modes of the bonds in the structural units, ZnO_4 , FeO_4 , BO_3 , and BO_4)
	Fe0	Fe2	Fe4	Fe6	Fe8	
1	400 >	400 >	400 >	400 >	400 >	stretching of Li-O bond [8].
2	554	550	545	550	553	Zn-O bending in ZnO_4 [22].
3	640	620	623	616	617	Overlap of Fe-O stretching in FeO_4 [24,26,27] with B-O-B bending in BO_3 as well as deformation modes of borate rings [4,21].
4	690	690	690	691	691	B-O-B symmetric bending in BO_3 [4,23].
5	860	863	863	867	870	B-O stretching of (NBOs) in BO_4 [20,23].
6	909	919	923	930	932	B-O stretching in BO_4 [3,24,25].
7	988	995	999	1002	1007	B-O stretching in BO_4 [3,20,24,25].
8	1069	1070	1072	1072	1073	B-O stretching in BO_4 [3,20,24,25].
9	1238	1238	1235	1236	1239	B-O asymmetric stretching of (NBOs) in BO_3 [23].
10	1300	1299	1300	1300	1301	B-O asymmetric stretching in BO_3 [3,9,20,22,23].
11	1366	1362	1363	1363	1365	B-O asymmetric stretching in BO_3 [3,22,23].
12	1460	1448	1445	1445	1445	B-O asymmetric stretching in BO_3 [3,22,23].
N_4	0.5084	0.4761	0.4689	0.4639	0.4603	

± 0.00015

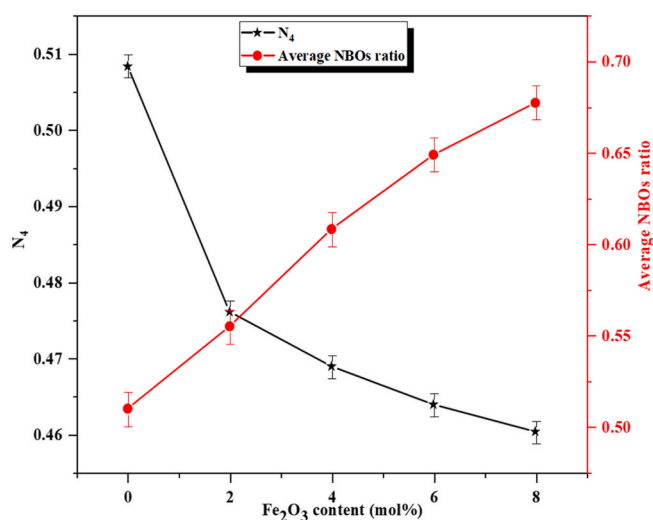


Fig. 3. Variation of N_4 and average NBOs ratio vs. Fe_2O_3 content.

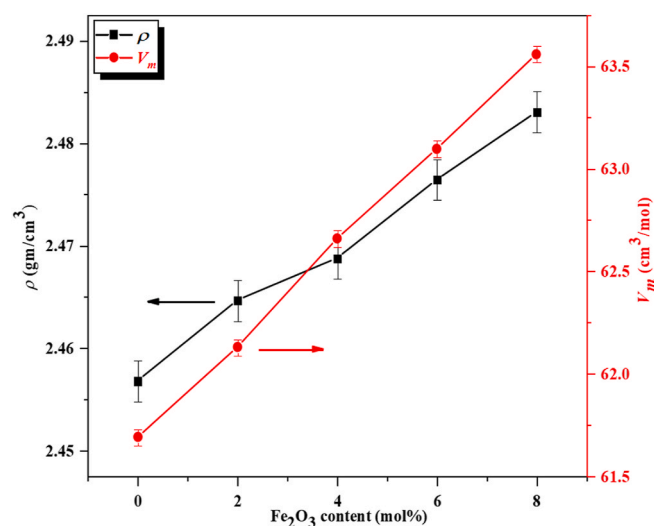


Fig. 4. Density and molar volume vs. Fe_2O_3 content.

Fe_2O_3 content. Increasing V_m with introducing Fe_2O_3 inside the glass matrix is may be due to the atomic radius of Fe cation (2.26 \AA) is larger than that of Zn cation (2.22 \AA) [29]. As well as, the reduction of N_4 ratio (i.e. transformation the glass network from closed structure to opened structure by conversion bridging oxygen's (BOs) in borate rings to NBOs). In this study, both of ρ and V_m increase as Fe_2O_3 content increase. This behavior may be a result of the increase in M_T is larger than that of ρ . V_m and ρ values were mentioned in Table 2 and shown in Fig. 4. Some other physical parameters were estimated such as ions concentration of Fe (N), inter atomic distance of Fe ions (R_i), polaron radius of Fe ions (r_p), field strength of Fe ions (F), and the average boron-boron separation (d_{B-B}) of the Fe glasses were computed using formulas [28,30], and the computed values were listed in Table 2.

$$N = \%mol \text{ of Fe } \frac{\rho N_A}{M_T} \quad (3)$$

$$R_i = \frac{1}{(N)^{1/3}} \quad (4)$$

$$r_p = \left(\frac{1}{2}\right) \left(\frac{\pi}{6N}\right)^{1/3} \quad (5)$$

$$F = \frac{Z}{r_p^2} \quad (6)$$

Table 2

Density (ρ), molar volume (V_M), Ions concentration of Fe (N), inter atomic distance of Fe (R_i), polaron radius of Fe (r_p), field strength of Fe (F), and the average boron-boron separation (d_{B-B}) For the glass samples.

Sample code	ρ (g/cm^3) ± 0.0037	V_M (cm^3/mol) ± 0.0034	N ($\times 10^{20}$ ions/ cm^3) $\pm 3.4 \times 10^{17}$	R_i (nm) $\pm 1.1 \times 10^{-3}$	r_p (nm) $\pm 1.1 \times 10^{-4}$	F ($\times 10^{16}$ cm^{-2}) $\pm 2.3 \times 10^{13}$	d_{B-B} (nm) ± 0.001
Fe0	2.457	61.689	0	–	–	–	0.5040
Fe2	2.465	62.128	1.939	1.728	0.696	1.151	0.5052
Fe4	2.469	62.659	3.844	1.375	0.554	1.818	0.5067
Fe6	2.476	63.097	5.727	1.204	0.485	2.371	0.5078
Fe8	2.483	63.560	7.580	1.097	0.442	2.858	0.5091

$$V_m^B = \frac{V_m}{2(1 - X_B)} \quad (7)$$

$$d_{B-B} = \left(\frac{V_m^B}{N_A}\right)^{1/3} \quad (8)$$

where N_A , Z , V_m^B , X_B are Avogadro's number, atomic mass of Fe, V_m^B molar volume of boron atoms and molar fraction of B_2O_3 , respectively.

3.3. Optical properties

Fig. 5 (a) shows the absorption spectra of all prepared glass samples. It is clearly that, these spectra exhibit some optical features such as the absorption edges and characteristic absorption bands. The absorption edges move towards the higher wavelength (i.e., red shift) as Fe_2O_3 content increases. The non-sharp absorption edges for all the samples indicate the non-crystalline nature for the glassy samples [28]. The spectra were deconvoluted to remove the overlapping between the absorption edge and absorption bands [23]. The deconvolution process produced six Gaussian peaks as shown in Fig. 5 (b). The first at 396.5 nm (ν_6), the second at ~ 436 nm (ν_5), the third at ~ 493 nm (ν_4), and fourth at ~ 596 nm (ν_3), these peaks attributed to ligand field transitions from the ground state to excitation states ${}^6A_1(6s) \rightarrow {}^4T_2(4D)$, ${}^6A_1(6s) \rightarrow {}^4A_1, {}^4E(4G)$, ${}^6A_1(6s) \rightarrow {}^4T_2(4G)$, and ${}^6A_1(6s) \rightarrow {}^4T_1(4G)$, respectively, which

refer to the characteristic absorption of Fe^{3+} ions in the UV-VIS regions that occupy sites with Td coordination [31–34]. The fifth peak at ~ 735 nm (ν_2) and the sixth peak at ~ 889 nm (ν_1) are related to the $Fe^{3+} {}^6A_1g(6s) \rightarrow {}^4T_2g(4G)$ [35] and ${}^6A_1g(6s) \rightarrow {}^4T_1g(4G)$ [31,32] transitions in Oh coordination, respectively. The increasing in intensities and area of Td transitions peaks and the decreasing in intensities and area of Oh transitions peaks are in accord with increasing of Fe^{3+} concentration in Td sites and decreasing of Fe^{3+} concentration in Oh sites in Mössbauer results. The 10Dq, B and C were estimated through peak centers in energy units of cm^{-1} and Tanabe-Sugano expressions for the ligand field state energies of Td Fe^{3+} , which are summarized in Table 3. The energies of first and second states which contain B^2 describe the configurational interaction were calculated assuming $C = 4B$. The quantities specified by \times in the ${}^4T_2(4D)$ state energy is neglected in the calculation of the spectroscopic state [12,36]. The estimation of B and C through the two transitions ${}^6A_1(6s) \rightarrow {}^4T_2(4D)$ and ${}^6A_1(6s) \rightarrow {}^4A_1, {}^4E(4G)$ is relatively straightforward where the two transitions are unaffected by 10Dq. The equations of the two transitions in terms of B and C are as follows:

$${}^6A_1(6s) \rightarrow {}^4T_2(4D) = 13B + 5C \sim \nu_6 \quad (9)$$

$${}^6A_1(6s) \rightarrow {}^4A_1, {}^4E(4G) = 10B + 5C \sim \nu_5 \quad (10)$$

where ν_4 , ν_3 are the approximate peak wavenumbers of the two transitions. From solution of the two equations of the two transitions in terms of B, C and approximate wavenumbers, we can get:

$$B = (\nu_6 - \nu_5)/3 \quad (11)$$

$$C = (13\nu_5 - 10\nu_6)/15 \quad (12)$$

Moreover, 10Dq was estimated from ${}^6A_1(6s) \rightarrow {}^4T_2(4G)$ transition, as shown in equation (13):

$${}^6A_1(6s) \rightarrow {}^4T_2(4G) = -10Dq + 18B + 6C - 38B^2/10Dq \sim \nu_4 \quad (13)$$

Equations (11)–(13) are very important mathematical equations which contribute in calculating the ligand field parameters of Fe^{3+} ions, and aiding the interested researchers in future to study the ligand field of Fe^{3+} ions by using these equations. The expansion of the electron cloud or the nephelauxetic effect (h) was calculated according to the expression:

$$h = \frac{[(B_0 - B)/B_0]}{k_{Fe^{3+}}} \quad (14)$$

where k and B_0 are central metal ion and Racah parameter for free Fe^{3+} ion, respectively [23,37]. For Fe^{3+} ion, $k = 0.24$ and $B_0 = 1015 \text{ cm}^{-1}$ [37, 38]. The values of 10D, B, C, C/B and h are reported in Table 4. The reported values of B and C decrease with increasing of Fe_2O_3 content as shown in Fig. 6. On the other hand, the 10Dq and h increase with increasing Fe^{3+} content as shown in Fig. 7. In the other words, the distance between 3d electrons of Fe^{3+} ion increases, and 3d orbitals become bigger and more diffused. Consequently, the inter-electronic repulsion Racah parameter (B) decreases, and the h increases [37]. B is an indicator of covalent nature of Fe^{3+} – ligand bonding, where the covalency increases when B decreases. The increase in h value means increasing the delocalization of d-electrons of Fe^{3+} ion [39]. The increasing of the delocalized electrons caused a red shift of the optical

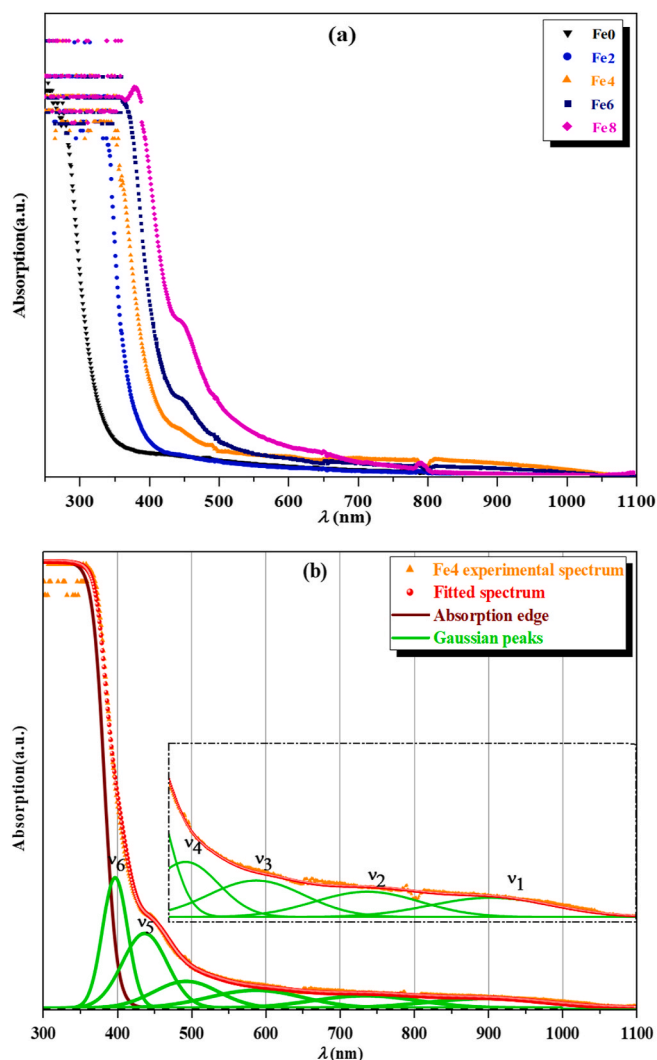


Fig. 5. UV-Vis absorption spectra of all prepared glass samples (a) and the deconvolution process of Fe4 sample (b).

Table 3
Tanabe-Sugano expressions of ligand field state energies of tetrahedral Fe^{3+} .

State	Configuration	Energy
${}^4T_1(4G)$	$(t_2)^4(e)^1$	$-10Dq + 10B + 6C - 26B^2/10Dq$
${}^4T_2(4G)$	$(t_2)^4(e)^1$	$-10Dq + 18B + 6C - 38B^2/10Dq$
${}^4A_1, {}^4E(4G)$	$(t_2)^3(e)^2$	$10B + 5C$
${}^4T_2(4D)$	$(t_2)^3(e)^2$	$13B + 5C \times$
${}^6A_1(6s)$	$(t_2)^3(e)^2$	0

Table 4

The ligand field strength (10Dq), Racah parameters B, C, ratio of C/B, nephelauxetic effect (h), Optical band gap (E_{opt}), refractive index (n_r), dielectric constant (ϵ), molar refraction (R_m), and the Molar polarizability (α_m) for the glass samples.

Sample code	10Dq (cm^{-1}) ± 2.4	B (cm^{-1}) ± 1.1	C (cm^{-1}) ± 2.2	C/B ± 0.008	h ± 0.004	E_{opt} (eV) ± 0.0006	n_r ± 0.0007	ϵ ± 0.001	R_m (cm^3/mol) ± 0.002	α_m ($\times 10^{-24} \text{cm}^3$) $\pm 1.8 \times 10^{-27}$
Fe0	–	–	–	–	–	3.6133	1.4950	2.235	18.051	7.153
Fe2	9172	771	3099	4.022	1.004	3.0600	1.4959	2.238	18.146	7.190
Fe4	9399	769	3040	3.955	1.012	2.9857	1.4964	2.239	18.316	7.258
Fe6	9587	765	3036	3.970	1.027	2.9277	1.4973	2.242	18.472	7.320
Fe8	9719	763	3005	3.941	1.036	2.8770	1.4980	2.244	18.632	7.383

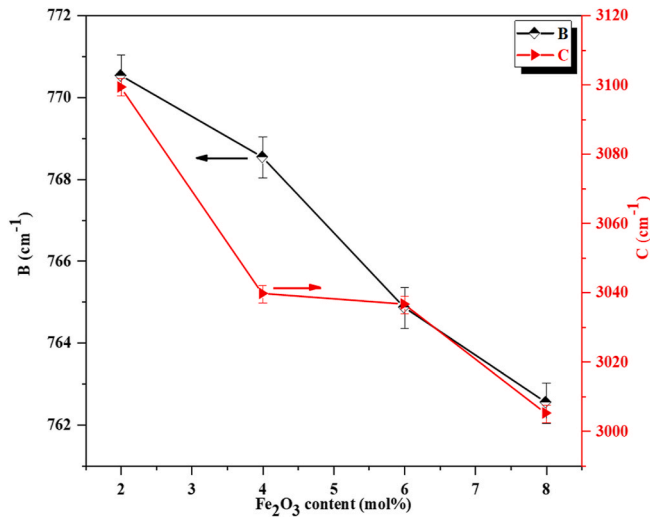


Fig. 6. Racah parameters (B and C) vs. Fe_2O_3 content.

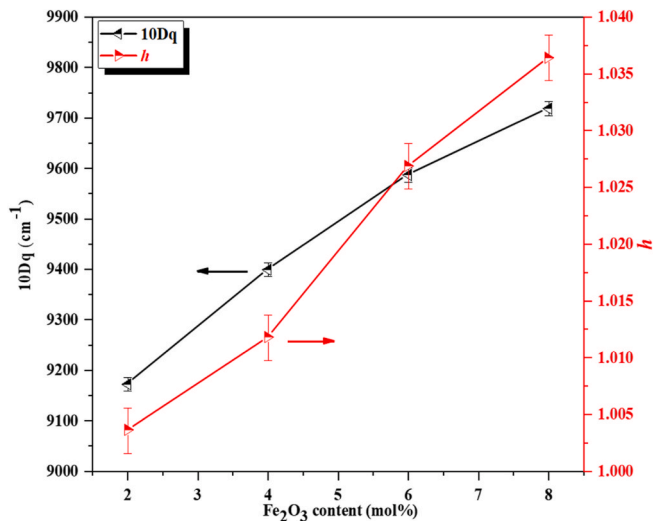


Fig. 7. The ligand field strength (10Dq) and nephelauxetic effect (h) vs. Fe_2O_3 content.

transitions and reduced the B values [40] as shown in Fig. 6. Optical absorption coefficient $\alpha(\nu)$ was evaluated by relation [41]:

$$\alpha(\nu) = 2.303(A/d) \quad (15)$$

where A and d are the absorbance and thickness of the sample, respectively.

The optical energy gap (E_{opt}) can be evaluated through general relation [4,8]:

$$ah\nu = B(h\nu - E_{opt})^b \quad (16)$$

where $h\nu$ and B are the incident photon energy and band tailing parameter, respectively. The index b equal 2, 1/2, 3, or 2/3 according to the type of electronic transition, indirect allowed, direct allowed, indirect forbidden, and direct forbidden transition, respectively [4,8]. The most possible transition in non-crystalline materials such as the glass is indirect allowed transition [41]. The E_{opt} for Fe glasses was evaluated by sketching $(ah\nu)^{1/2}$ vs. $h\nu$ and extrapolating the linear part of the of $(ah\nu)^{1/2}$ vs. $h\nu$ at $(ah\nu)^{1/2}$ equal zero (not shown) [41]. The evaluated values are mentioned in Table 4. E_{opt} of Fe glass samples reduces step by step as Fe_2O_3 content increase as illustrated in Fig. 8 this decrement is owing to an enhancement of NBOs bonds in glass matrix whenever Fe_2O_3 content increases [4]. The excited electrons existing in NBOs need to less energy than the electrons existing in BOs. Because of, NBOs have electrons with less bound than which in BOs [42]. Subsequently, an increasing NBOs leads to decreasing in the E_{opt} . Refractive index (n_r) of glasses with density located between 1 and 3 g/cm^{-3} , the dielectric constant (ϵ), the molar refraction (R_m) and the Molar polarizability (α_m) are estimated from the following equations [43,44] and reported in Table 4.

$$n_r = \frac{\rho + 10.4}{8.6} \quad (17)$$

$$\epsilon = n_r^2 \quad (18)$$

$$R_m = \frac{V_m(n_r^2 - 1)}{(n_r^2 + 2)} \quad (19)$$

$$R_m = \frac{4\pi N_A \alpha_m}{3} \quad (20)$$

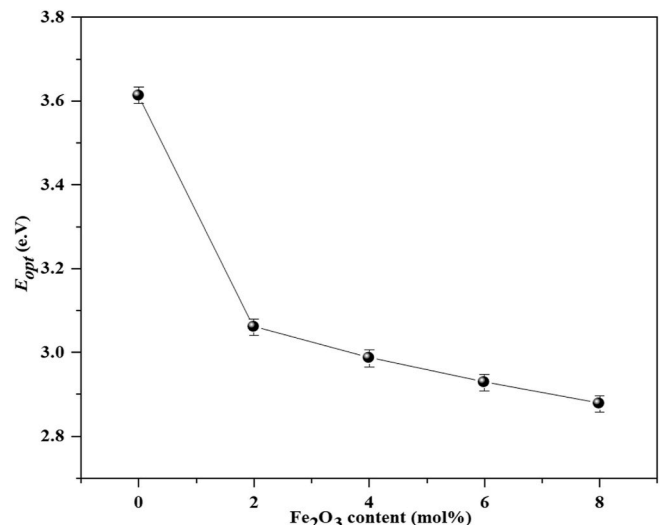


Fig. 8. Optical band gap E_{opt} vs. Fe_2O_3 content.

$$\alpha_m = \frac{3R_m}{4\pi N_A} \quad (21)$$

3.4. ESR spectroscopy

The ESR spectra of Fe glasses at RT are shown in Fig. 9. The ESR spectra of free Fe glass sample have not shown any absorption indicating that, the sample is free from Fe^{3+} ions. When iron ions are introduced in the glasses the spectra exhibited a resonance signal at $g \sim 2.1$, sharp signal at $g \sim 4.1$ and tiny shoulder (kink) at $g \sim 6.7$ in the all doped samples. The signal at $g \sim 2.1$ is attributed to a two superimposed lines pattern consisting of a broad line and a narrow line are resulted from a cooperation of two types of Fe^{3+} ion pairs, the broad line is caused by pairs or clusters of exchange-coupled Fe^{3+} , while the narrow line is due to microclusters with smaller distances between the paramagnetic ions [45,46] in distorted octahedral (tetrahedral) sites [1,47]. The signal at $g \sim 4.1$ attributed to distribution of the isolated Fe^{3+} ions mainly located in rhombically distorted Td or Oh Oxygen environments [10,15,48]. The signal at $g \sim 6.7$ attributed to axially distorted sites [48,49]. The intensity of the absorption line located at $g \sim 2.1$ increases while the intensities of the lines centered at $g \sim 4.1$ and ~ 6.7 decrease whenever Fe_2O_3 content increases. The decrement in the intensity of the resonance line centered at $g \sim 4.1$ is due to devastation of the neighbors configuration in the Fe ions vicinity, whereas the increasing of Fe_2O_3 density in the glass network destroys the local ordering of the Fe^{3+} ions vicinities [1,48]. Consequently, the percentage of the isolated Fe^{3+} ions in the Td or Oh oxygen environments decreases and the line intensity that located at $g \sim 4.1$ decreases [1,10,48]. The decrement in the intensity of the resonance line centered at $g \sim 4.1$ is accompanied by the increment in the intensity of the resonance line centered at $g \sim 2.1$ with increasing of Fe_2O_3 content. This behavior may be attributed to that at lower concentration of Fe_2O_3 , iron positions are inhabited randomly in the glass network but at higher concentration of Fe_2O_3 diverts from randomness to formation the clusters [1,10].

3.5. Mössbauer spectroscopy

The obtained Mössbauer spectra of the iron doped glass samples are shown in Fig. 10. Mössbauer's parameters of the hyperfine interaction were analyzed and extracted by a computer program depended on Voigt profile. Table 5 shows Mössbauer's parameters, isomer shift (IS), quadrupole splitting (QS), widths of Gaussian distribution (GW), concentration of Fe^{3+} ions in Oh sites % ($\text{Fe}^{3+}_{\text{Oh}}$ %), and concentration of Fe^{3+} ions in Td sites % ($\text{Fe}^{3+}_{\text{Td}}$ %) of the samples doped with iron. The

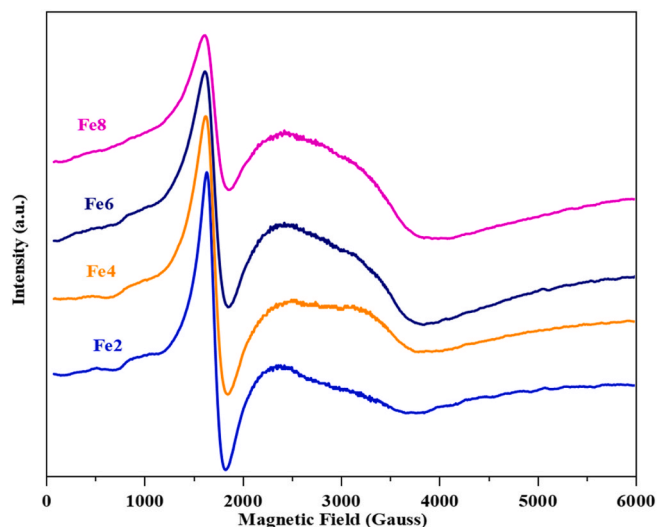


Fig. 9. ESR spectra of doped glass samples.

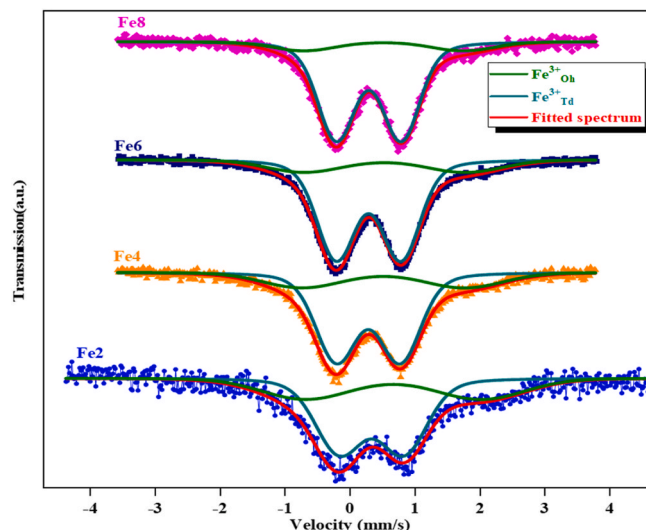


Fig. 10. Mössbauer spectra of doped glass samples.

tabulated data show two phases of iron ions existing in the glass network, the first is related to Fe^{3+} ions in Oh sites with the isomer shift ($0.675\text{--}0.553$) mm s^{-1} [50], the second is related to Fe^{3+} ions in Td sites with the isomer shift below 0.34 mm s^{-1} [51]. The IS and QS of the first phase ($\text{Fe}^{3+}_{\text{Oh}}$) decrease with increasing Fe_2O_3 content at the expense of ZnO, in contrast to the second phase ($\text{Fe}^{3+}_{\text{Td}}$). The decreasing in IS and QS of $\text{Fe}^{3+}_{\text{Oh}}$ can be interpreted in terms of increase of NBOs with increasing Fe_2O_3 content. In the oxide glass, the electrons of the NBOs have energy levels higher than energy levels of BOs. Subsequently, the chemical bond between NBOs and boron is weaker than that between BOs and boron. As well as, Coulombic interaction between NBOs and Fe^{3+} ions is stronger than that between BOs and Fe^{3+} ions. Therefore, the oxygen atoms of NBOs are closer to $\text{Fe}^{3+}_{\text{Oh}}$ than the oxygen atoms of BOs lead to overlap of 4s orbitals of $\text{Fe}^{3+}_{\text{Oh}}$ with the 2p orbitals of NBOs. As a result, the s-electron density at $\text{Fe}^{3+}_{\text{Oh}}$ nucleus increases and IS of $\text{Fe}^{3+}_{\text{Oh}}$ decreases [52,53]. In addition, the decreasing of the distance between NBO and $\text{Fe}^{3+}_{\text{Oh}}$ increases the symmetry around $\text{Fe}^{3+}_{\text{Oh}}$ and decreases the QS [53]. The increasing in IS and QS of $\text{Fe}^{3+}_{\text{Td}}$ indicated that, a decrease in the s-electron density at $\text{Fe}^{3+}_{\text{Td}}$ nucleus and the surroundings of $\text{Fe}^{3+}_{\text{Td}}$ becomes less symmetrical as Fe_2O_3 content increases, respectively.

4. Conclusions

The analysis of IR spectra of the Fe glass samples indicates the presence of characteristic borate structural units (BO_4 , BO_3 , and NBOs), addition of iron ions seem to cause change in the disorder structure of glass matrix by transformation of BO_4 to BO_3 and creating of NBOs, decreasing of N_4 values ($0.5084 - 0.4603$) indicate increased NBOs concentration with increased iron content. The increasing of density ($2.457 - 2.483$ g/cm^3) and molar volume ($61.689 - 63.560$ cm^3/mol) may be due to converting the glass network structure from close structure to open structure and the increase in molecular weight of composition as the concentration of Fe_2O_3 increase. 10Dq , B and C have been evaluated. 10Dq increases ($9172 - 9719$ cm^{-1}), while B decreases ($771 - 763$ cm^{-1}) and C decreases ($3099 - 3005$ cm^{-1}) with increasing of Fe_2O_3 content. The increasing of Fe_2O_3 concentration in the composition lead to increasing number of NBOs and decreasing of E_{opt} ($3.6133 - 2.8770$ eV) where excitation electron that in NBOs need less energy than that in BOs. ESR spectra show existence Fe^{3+} ions in all Fe_2O_3 doped glass samples in form isolated Fe^{3+} ions characteristic by absorption line at $g \sim 4.1$ and in form Fe^{3+} clusters/microclusters characteristic by two superimposed lines at $g \sim 2.1$. Existence ratio of Fe^{3+} in form isolated Fe^{3+} ions or Fe^{3+} clusters/microclusters and intensity of absorption lines

Table 5

Mössbauer's parameters of the iron doped glasses samples, isomer shift (IS), quadrupole splitting (QS), widths of Gaussian distribution (GW), concentration of Fe³⁺ ions in octahedral sites % (Fe³⁺_{Oh} %), and concentration of Fe³⁺ ions in tetrahedral sites % (Fe³⁺_{Td} %).

Sample code	Fe ³⁺ _{Oh}			Fe ³⁺ _{Td}			Fe ³⁺ _{Oh} %	Fe ³⁺ _{Td} %
	IS (mm s ⁻¹)	QS (mm s ⁻¹)	GW (mm s ⁻¹)	IS (mm s ⁻¹)	QS (mm s ⁻¹)	GW (mm s ⁻¹)		
Fe2	0.675	2.707	0.621	0.339	0.991	0.316	33.1	66.9
Fe4	0.554	2.667	0.587	0.31	1.045	0.288	23.6	76.4
Fe6	0.552	2.638	0.563	0.312	1.06	0.265	18.8	81.2
Fe8	0.553	2.615	0.465	0.316	1.062	0.254	13.2	86.8

depending on the concentration of Fe₂O₃ in the glass samples. Mössbauer spectra reveal two phases of Fe ions, Fe³⁺_{Oh} with IS decreases (0.675–0.553 mm s⁻¹) with increasing Fe₂O₃ content and Fe³⁺_{Td} with IS below 0.34 mm s⁻¹.

CRedit authorship contribution statement

Essam A. Elkelany: Writing - original draft. **Moukhtar A. Hassan:** Conceptualization, Formal analysis. **A. Samir:** Writing - original draft. **A.M. Abdel-Ghany:** Resources. **H.H. El-Bahnasawy:** Writing - review & editing. **M. Farouk:** Supervision.

Declaration of competing interest

The authors declare that they have no known competing financial interests or personal relationships that could have appeared to influence the work reported in this paper.

References

- I. Ardelean, R. Lungu, P. Pascuta, EPR and magnetic susceptibility studies of iron ions in 3B2O3-SrO glass matrix, *J. Optoelectron. Adv. Mater.* 10 (2008) 1306–1310.
- N. Deopa, S. Saini, S. Kaur, A. Prasad, A.S. Rao, Spectroscopic investigations on Dy³⁺ ions doped zinc lead alumino borate glasses for photonic device applications, *J. Rare Earths* 37 (2019) 52–59, <https://doi.org/10.1016/j.jre.2018.04.013>.
- E. Mansour, FTIR spectra of pseudo-binary sodium borate glasses containing TeO₂, *J. Mol. Struct.* 1014 (2012) 1–6, <https://doi.org/10.1016/j.molstruc.2012.01.034>.
- M.G. Moustafa, M.Y. Hassaan, Optical and dielectric properties of transparent ZrO₂-TiO₂-Li₂B₄O₇ glass system, *J. Alloys Compd. J.* 710 (2017) 312–322, <https://doi.org/10.1016/j.jallcom.2017.03.192>.
- E. Ekdal, T. Karali, A. Kelemen, V. Holovey, M. Ignatovych, Evaluation of kinetic parameters of Li₂B₄O₇: Mn single crystal, *J. Alloys Compd.* 588 (2014) 413–417.
- A.A. Abul-magd, H.Y. Morshidy, A.M. Abdel-Ghany, The role of NiO on the structural and optical properties of sodium zinc borate glasses, *Opt. Mater.* 109 (2020), <https://doi.org/10.1016/j.optmat.2020.110301>, 110301.
- H. Gui, C. Li, C. Lin, Q. Zhang, Z. Luo, L. Han, J. Liu, T. Liu, A. Lu, Glass forming, crystallization, and physical properties of MgO-Al₂O₃-SiO₂-B₂O₃ glass-ceramics modified by ZnO replacing MgO, *J. Eur. Ceram. Soc.* 39 (2019) 1397–1410, <https://doi.org/10.1016/j.jeurceramsoc.2018.10.002>.
- N. Elkhoshkhany, S.Y. Marzouk, M.A. Khattab, S.A. Dessouki, Influence of Sm₂O₃ addition on Judd-Ofelet parameters, thermal and optical properties of the TeO₂-Li₂O-ZnO-Nb₂O₅ glass system, *Mater. Char.* 144 (2018) 274–286, <https://doi.org/10.1016/j.matchar.2018.07.021>.
- S. Prakash, R.P.S. Chakradhar, J.L. Rao, B. Karmakar, EPR, FTIR, optical absorption and photoluminescence studies of Fe₂O₃ and CeO₂ doped ZnO-Bi₂O₃-B₂O₃ glasses, *J. Alloys Compd. J.* 493 (2010) 256–262, <https://doi.org/10.1016/j.jallcom.2009.12.075>.
- R.K. Singh, G.P. Kothiyal, A. Srinivasan, Electron spin resonance and magnetic studies on CaO-SiO₂-P₂O₅-Na₂O-Fe₂O₃ glasses, *J. Non-Cryst. Solids* 354 (2008) 3166–3170, <https://doi.org/10.1016/j.jnoncrystol.2008.01.009>.
- R.G. Burns, MINERALOGICAL APPLICATIONS OF CRYSTAL FIELD THEORY, 1993.
- D.M. Sherman, A.T. David Waite, Electronic spectra of Fe³⁺ oxides and oxide hydroxides in the near IR to near UV, *Am. Mineral.* 70 (1985) 1262–1269.
- P.A. Bingham, J.M. Parker, T. Searle, J.M. Williams, I. Smith, Novel structural behaviour of iron in alkali - alkaline-earth, - silica glasses 5 (2002) 787–796.
- J. House, Inorganic Chemistry, third ed., Elsevier Inc, 2020 <https://doi.org/10.1016/B978-0-12-814369-8.00017-0>.
- S.T. dos Reis, W.M. Pontuschka, J.B. Yang, D.L.A. Faria, Properties and structural features of iron doped BABAL glasses, *Mater. Res.* 6 (2003) 389–394.
- P.G. Pavani, M. Prasad, V.C. Mouli, DSC, ESR and optical absorption studies of Cu²⁺ ion doped in boro cadmium tellurite glasses, *J. Alloy. Compd. Jou.* 527 (2012) 5–9, <https://doi.org/10.1016/j.jallcom.2012.02.142>.
- Brent Fultz, Mössbauer Spectrometry, in: Elton Kaufmann (Ed.), Characterization of Materials, John Wiley, New York, 2011 (n.d.).
- K. Tanaka, K. Hirao, N. Soga, Mossbauer study OF sodium iron borate glasses, *J. Non-Cryst. Solids* 85 (1986) 228–232.
- T. Nishida, Advances in the Mossbauer effect for the structural study of glasses, *J. Non-Cryst. Solids* 177 (1994) 257–268.
- M. Farouk, Effect of Co²⁺ ions on the ligand field, optical, and structural properties of ZnLiB glasses, *Optik* 140 (2017) 186–196.
- A.M. Abdelghany, M.A. Ouis, M.A. Azooz, H.A. Elbatal, G.T. El-bassyouni, Role of SrO on the bioactivity behavior of some ternary borate glasses and their glass ceramic derivatives, *Spectrochim. ACTA PART A Mol. Biomol. Spectrosc.* 152 (2016) 126–133, <https://doi.org/10.1016/j.saa.2015.07.072>.
- A. Samir, M.A. Hassan, L.I. Soliman, M. Elok, Characterization of borate glasses doped with copper oxide for optical application, *Opt. Quant. Electron.* (2019) 1–13.
- M.A. Hassan, F.M. Ebrahim, M.G. Moustafa, Z.M.A. El-fattah, M.M. El-okr, Unraveling the hidden Urbach edge and Cr⁶⁺ optical transitions in borate glasses, *J. Non-Cryst. Solids J.* 515 (2019) 157–164, <https://doi.org/10.1016/j.jnoncrystol.2019.02.026>.
- P. Pascuta, R. Lungu, I. Ardelean, FTIR and Raman spectroscopic investigation of some strontium - borate glasses doped with iron ions, *J. Mater. Sci. Mater. Electron.* 21 (2010) 548–553, <https://doi.org/10.1007/s10854-009-9955-7>.
- M.Ş. Todera, S. Filip, I. Ardelean, Structural study of the Fe₂O₃-B₂O₃-BaO glass system by FTIR spectroscopy, *J. Optoelectron. Adv. Mater.* 8 (2006) 1121–1123.
- E.K. Abdel-Khalek, E.A. Mohamed, S.M. Salem, I. Kashif, Structural and dielectric properties of (100-x)B₂O₃-(x/2)Bi₂O₃-(x/2) Fe₂O₃ glasses and glass-ceramic containing BiFeO₃ phase, *J. Non-Cryst. Solids* 492 (2018) 41–49, <https://doi.org/10.1016/j.jnoncrystol.2018.04.020>.
- E. El-meliqy, M. Mabrouk, S.A.M. El-sayed, B.M.A.E. Hady, M.R. Shehata, W. M. Hosny, Novel Fe₂O₃-Doped Glass/chitosan Scaffolds for Bone Tissue Replacement vol. 44, 2018, pp. 9140–9151.
- P. Chimalawong, J. Kaewkhao, C. Kedkaew, P. Limsuwan, Optical and electronic polarizability investigation of Nd³⁺ -doped soda-lime silicate glasses, *J. Phys. Chem. Solid.* 71 (2010) 965–970, <https://doi.org/10.1016/j.jpcs.2010.03.044>.
- M. Rahm, R. Hoffmann, N.W. Ashcroft, Atomic and ionic radii of elements 1 – 96, *Chemistry* (2016) 14625–14632, <https://doi.org/10.1002/chem.201602949>.
- H.Y. Morshidy, M.S. Sadeq, Influence of Cobalt Ions on the Structure, Phonon Emission, Phonon Absorption and Ligand Field of Some Sodium Borate Glasses, 2019, p. 525.
- B. Hannyer, M. Lenglet, J. DiJrr, R. Cortes, Spectroscopic evidence of octahedral iron (III) in soda-lime silicate glasses, *J. Non-Cryst. Solids* 151 (1992) 209–216.
- L. Alyabyeva, V. Burkov, B. Mill, Optical spectroscopy of La₃Ga₅SiO₄ disordered crystals doped with Fe³⁺ ions, *Opt. Mater.* 43 (2015) 55–58, <https://doi.org/10.1016/j.optmat.2015.02.023>.
- V. Vercamer, G. Lelong, H. Hijjiya, Y. Kondo, L. Galoisy, G. Calas, Diluted Fe³⁺ in silicate glasses: structural effects of Fe-redox state and matrix composition. An optical absorption and X-band/Q-band EPR study, *J. Non-Cryst. Solids* 428 (2015) 138–145, <https://doi.org/10.1016/j.jnoncrystol.2015.08.010>.
- Y. Wang, R.K. Li, d-d Transitions of Fe³⁺ ions in Fe-doped K₂Al₂B₂O₇ crystal, *Opt. Mater.* 32 (2010) 1313–1316, <https://doi.org/10.1016/j.optmat.2010.04.036>.
- M. Lenglet, F. Hochu, Z. Simsa, COVALENCY OF Fe³⁺-O₂- BONDS AND MAGNETIC STRUCTURE IN MIXED OXIDES, *Mater. Res. Bull.* 33 (1998) 1821–1833.
- A. Lever, Inorganic Electronic Spectroscopy, Elsevier, 1984.
- M. Gerloch, E.G. Constable, Transition Metal Chemistry, 1994.
- A.L. Tchougreeff, R. Dronskowski, Nephelauxetic Effect Revisited 109 (2009) 2606–2621, <https://doi.org/10.1002/qua>.
- G. Giridhar, S.S. Sastry, M. Rangacharyulu, Spectroscopic studies on Pb₃O₄-ZnO-P₂O₅ glasses doped with transition metal ions, *Phys. B.* 406 (2011) 4027–4030, <https://doi.org/10.1016/j.physb.2011.07.024>.
- J. Maria Neto, T. Abritta, F. Barros, N. Melamed, A COMPARATIVE STUDY OF THE OPTICAL PROPERTIES OF Fe³⁺ IN ORDERED LiGa₅O₈ AND LiAl₅O₈, *J. Lumin.* 22 (1981) 109–120.
- M.S. Sadeq, M.A. Abdo, Effect of iron oxide on the structural and optical properties of alumino-borate glasses, *Ceram. Int.* 47 (2) (15 January 2021) 2043–2049, <https://doi.org/10.1016/j.ceramint.2020.09.036>.
- E. Sayed, S.F. Mansour, M.Y. Hassaan, A.M. Emara, Synthesis optical properties of novel TeO₂ based glasses, *Optik* 127 (2016) 8933–8939.
- S. Dalal, S. Khasa, M.S. Dahiya, A. Yadav, A. Agarwal, S. Dahiya, Optical and thermal investigations on vanadyl doped zinc lithium borate glasses, *J. Asian Ceram. Soc.* 3 (2015) 234–239.

- [44] A. Edukondalu, B. Kavitha, M.A. Samee, S. Kareem, S. Rahman, K.S. Kumar, Mixed alkali tungsten borate glasses – optical and structural properties, *J. Alloys Compd.* 552 (2013) 157–165, <https://doi.org/10.1016/j.jallcom.2012.10.010>.
- [45] R. Berger, J. Claude Bissey, J. Kliava, B. Soulard, Superparamagnetic resonance of ferric ions in devitrified borate glass, *J. Magn. Magn Mater.* 167 (1997).
- [46] R. Berger, J. Kliava, E. Yahiaoui, J. Bissey, P.K. Zinsou, P. Bziade, Diluted and Non-diluted Ferric Ions in Borate Glasses Studied by Electron Paramagnetic Resonance, vol. 180, 1995, pp. 151–163.
- [47] P. Pascuta, G. Borodi, A. Popa, V. Dan, E. Culea, Influence of iron ions on the structural and magnetic properties of some zinc-phosphate glasses, *Mater. Chem. Phys.* 123 (2010) 767–771, <https://doi.org/10.1016/j.matchemphys.2010.05.056>.
- [48] P.S. Rani, R. Singh, Electron spin resonance and magnetization studies of ZnO–TeO₂–Fe₂O₃ glasses, *J. Phys. Chem. Solid.* 74 (2013) 338–343.
- [49] H. Göktürk, MEASUREMENT OF TRANSITION METALS IN SODA-LIME-SILICATE GLASSES BY USING ELECTRON SPIN RESONANCE (ESR) SPECTROSCOPY, 2017.
- [50] A.F.L. Almeida, D. Thomazini, I.F. Vasconcelos, M.A. Valente, A.S.B. Sombra, Structural Studies of Lithium Triborate (LBO – LiB₃O₅) in Borophosphate Glass-Ceramics vol. 3, 2001, pp. 829–838.
- [51] M.Y. Hassaan, M.G. Moustafa, K. Osouda, S. Kubuki, T. Nishida, 57Fe and 119Sn Mossbauer, XRD, FTIR and DC conductivity study of Li₂O-Fe₂O₃-SnO₂-P₂O₅ glass and glass ceramics, *J. Alloys Compd. J.* 765 (2018) 121–127.
- [52] H.B. Pascoal, W.M. Pontuschka, H. Rechenberg, Investigation of Fe+3 and Fe+2 properties in calcium aluminoborate glasses 214 (2000) 211–214.
- [53] X. Ren, W. Zhang, Y. Zhang, P. Zhang, J. Liu, Effects of Fe₂O₃ content on microstructure and mechanical properties of CaO–Al₂O₃–SiO₂ system, *Trans. Nonferrous Metals Soc. China* 25 (2015) 137–145, [https://doi.org/10.1016/S1003-6326\(15\)63588-9](https://doi.org/10.1016/S1003-6326(15)63588-9).